COMPARISON OF PREDICTED ONSET OF FAILURE MECHANISMS BY NONLINEAR FAILURE THEORY AND BY ACOUSTIC EMISSION MEASUREMENTS

M. G. R. Sause[a*], A. Monden[a]

[a]*Experimental physics II, Institute for physics, University of Augsburg, D-86135 Augsburg*
**markus.sause@physik.uni-augsburg.de*

Keywords: Acoustic emission, failure criterion, fracture, polymer-matrix composites

Abstract
Tensile testing of carbon fiber reinforced polymer specimens with three different cross-ply stacking sequences was performed with simultaneous detection of acoustic emission signals. The detected signals were analyzed by pattern recognition methods to distinguish between the occurrence of matrix cracking, interfacial failure, and fiber breakage as a function of loading. The frequency of occurrence of failure mechanisms expected for the different stacking sequences of the laminates corresponded to the number and amplitude of respective acoustic emission signal clusters. The onset of the individual failure mechanisms was compared to analytical predictions from nonlinear analysis of laminate failure and was found to be in systematic agreement.

1. Introduction

Fiber-reinforced polymers are materials of great interest in modern lightweight engineering because they show extraordinary strength-to-weight and stiffness-to-weight ratios. In practice, the full potential of carbon-fiber-reinforced polymers (CFRP) is rarely used, because prediction of composite failure by reliable failure models is still an active field of research [1–4]. Several microscopic types of failure exist in CFRP, which ultimately result in complex macroscopic failure. The relevance of the various failure mechanisms to the composites integrity and stability depends on the application and type of loading. In order to understand the individual contributions of these failure mechanisms, it is vital to record their evolution as a function of loading.
In the past, various authors used acoustic emission analysis to detect the onset and position of microscopic failure occurring in fiber-reinforced materials and many attempts have been made to distinguish between different types of failure [5-11]. Most of the approaches for source identification rely on the propagation behavior of Lamb waves, which are typically found in flat (plate-like) CFRP specimens. For sufficiently thin plates (i.e. thickness < 5 mm) and frequency ranges below 1 MHz, only the zero-order symmetric (S_0) and zero-order antisymmetric (A_0) Lamb wave modes are encountered in acoustic emission testing. Various authors suggest to distinguish between fiber breakage and matrix cracking based on the significant contributions at high frequencies (fiber breakage) or low frequencies (matrix cracking) of the acoustic emission signals [6,8,9,11]. However, a significant shift of the weight of frequency distributions as a function of the distance between the acoustic emission source and the sensor position occurs [11,12]. To overcome this problem, parameter-based

pattern-recognition techniques can be applied to form more complex decision criteria to detect and separate clusters of acoustic emission signals originating from different microscopic failure mechanisms [7-11,13].

In this study, we follow the way of source identification based on finite element modeling of the acoustic emission source, signal propagation, and signal detection process [13,14]. Here the basis for distinguishing different microscopic failure mechanisms are the orientation of the crack surface displacement (in-plane or out-of-plane) and the elastic properties of the cracking medium (i.e. matrix or fiber). Thus, a prerequisite to source identification is the strict correlation between a characteristic source radiation pattern and a particular micromechanical failure mode. A precise description of the implementation used in the particular source types is found in Ref. [13] and is thus not repeated here. The description of mesoscopic failure modes (i.e., fiber bridging) is beyond the scope of the proposed acoustic emission source models.

Typical microscopic failure mechanisms occurring in tensile testing of cross-ply laminates are matrix cracking, fiber breakage, and interfacial failure (i.e., fiber-matrix debonding, fiber pull-out). Among the fracture mechanics theories for predicting laminate failure, Puck's failure criterion [1,4] is widely applied. In this approach, a distinction is made between the occurrence of interfiber fracture (IFF) and fiber fracture (FF). In the case of cross-ply laminates subject to tensile loading, IFF is correlated to the occurrence of matrix cracking (i.e., crack propagation within the matrix) or interfacial failure (i.e., crack propagation at the interface between fiber and matrix) in the plies with fiber orientation perpendicular to the load axis. After the initial formation of IFF, inter-ply delamination is likely to occur at the boundary between the 0° and 90° layers.
In the current study, we present the experimental setup used to obtain the acoustic emission data, discuss the experimental results and compare the measured onset of distinct acoustic emission source types to predictions of laminate failure calculated by the method of Puck et al. [1,4].

2. Experimental

All specimens investigated were prepared from the Sigratex CE 1250-230-39 unidirectional prepreg system with a 60% fiber-volume fraction. Specimens were manufactured under vacuum conditions using the curing cycle recommended by the material supplier (130 °C, 1.5 h, 0.4 bars) and were cut using an electrical tile cutter with diamond cutting wheel.
In order to perform a nonlinear analysis of laminate failure according to Puck et al. [1], the mechanical properties of the unidirectional laminate were measured as summarized in table 1. To calculate Puck's failure criterion, the software package AlfaLam.nl (Advanced layerwise failure analysis of Laminates.non-linear) was used. Stress exposure values were calculated for the 90° layers and for the 0° layers to derive the failure stress and failure strain for IFF and FF.

For the tensile tests, including the simultaneous acquisition of acoustic emission signals, different specimen types were prepared. Commonly used standards require reinforcement tabs glued to the specimen ends to ensure failure in the tapered section of the specimen. Often, the glue fails partially during specimen loading, which causes additional acoustic emission sources not related to the failure of the tensile specimen. In order to avoid this problem additional plies were inserted in 45°, 0°, and 135° orientation at the end section of the specimen to increase the thickness from 2.2 mm in the reduced section to 4.2 mm in the

tapered section (see Fig. 1). In the reduced section, three different stacking sequences of $[0/90/90/90/0]_{sym}$, $[0/0/90/90/0]_{sym}$, and $[0/0/90/0/0]_{sym}$ were prepared. The subscript "sym" indicates that the laminate is balanced (symmetric), i.e., the given stacking sequence is repeated in reverse order. The final dimensions of the test specimens were 180 ± 2 mm × 16.2 ± 0.5 mm (length × width) with a reduced section of 74 ± 1 mm × 2.2 ± 0.2 mm (length × thickness).

Property	Value	Standard
Parallel Young's modulus $E_{\parallel}$	128.7 [GPa]	DIN EN 2561
Parallel tensile strength $\sigma_{\parallel}^{t}$	1660 [MPa]	DIN EN 2561
Poisson's ratio $\nu_{\perp\parallel}$	0.33	DIN EN 2561
Transverse Young's modulus $E_{\perp}^{t}$	9.1 [GPa]	DIN EN 2597
Transverse tensile strength $\sigma_{\perp}^{t}$	54 [MPa]	DIN EN 2597
Parallel compressive strength $\sigma_{\parallel}^{c}$	703 [MPa]	ASTM D 6641
Transverse compressive strength $\sigma_{\perp}^{c}$	88 [MPa]	ASTM D 6641
In-plane shear modulus $G_{\perp\parallel}$	6.8 [GPa]	ASTM D 7078
In-plane shear strength $\sigma_{\perp\parallel}$	80 [MPa]	ASTM D 7078
Density ρ	1550 [kg/m³]	datasheet

Table 1: Measurement results for prepreg Sigratex CE 1250-230-39.

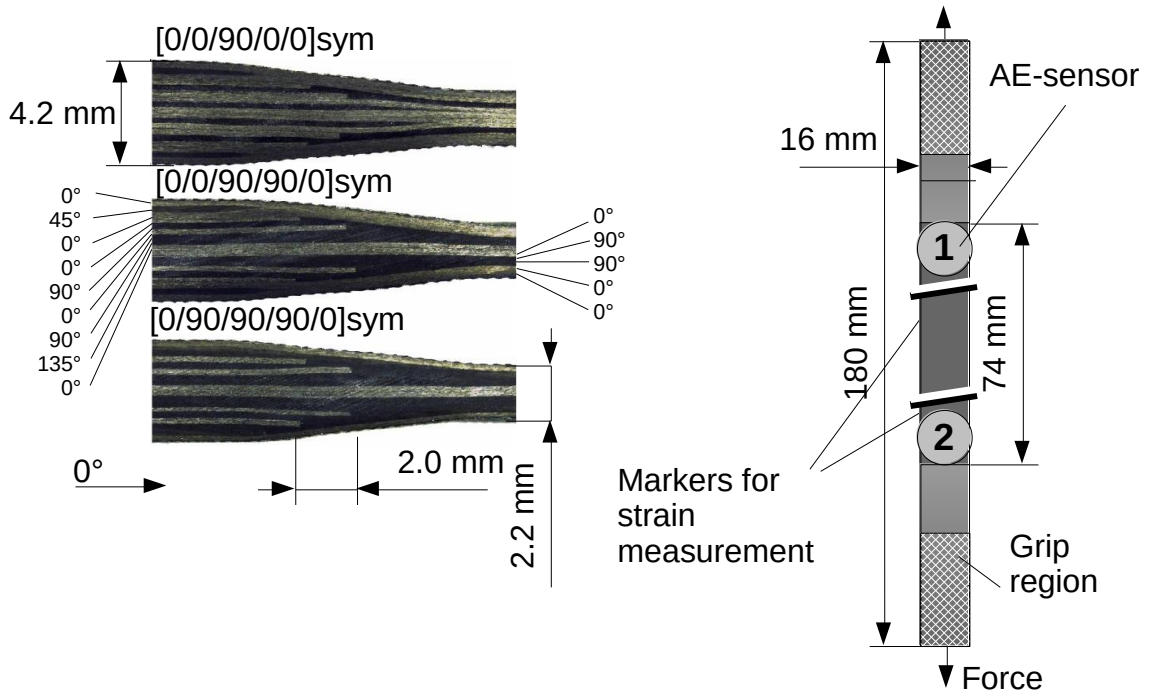

Figure 1. Cross-sectional images of reinforcement sections of the three stacking sequences investigated (left) and scheme of test configuration (right).

Seven specimens were tested for each stacking sequence using a Zwick 1464 spindle-driven machine at a displacement rate of 0.5 mm/min. The force was measured using a 50 kN load cell and the displacement was measured in the tapered region of the specimens by monitoring strain markers with a optical (contact-free) extensometer of the videoXtens type from Zwick.

Acoustic emission signals were recorded using a Physical Acoustic PCI-2 system with 2/4/6 preamplifiers and two WD AE sensors in linear geometry as illustrated in Fig. 1. The signals were detected with a threshold-based triggering mechanism using 10/80/300 µs (Peak-

Definition-Time/Hit-Definition-Time/Hit-Lockout-Time) at a threshold of 35 dB_{AE} and a preamplification of 20 dB, and were recorded with an acquisition rate of 10 MS/s and a band-pass filter ranging from 20 kHz to 1 MHz. Acoustic coupling was provided by a medium viscosity silicone grease, while the sensors were attached using suitable clamp systems to ensure a reproducible mounting pressure. Sensor coupling was validated by pulsing sensor 1 and the measurement of signal amplitudes at sensor 2. The sound velocity of the S_0 Lamb wave mode, required to calculate the source position, is determined from the measured time between pulsing sensor 1 and detection at sensor 2 and their metric distance of 56 mm between their centers. These are evaluated as 4814 ± 138 m/s, 4332 ± 285 m/s, and 4081 ± 278 m/s for the three stacking sequences of $[0/0/90/0/0]_{sym}$, $[0/0/90/90/0]_{sym}$, and $[0/90/90/90/0]_{sym}$. After signal acquisition, the acoustic emission source position was determined based on a Δt-localization technique using the linear sensor arrangement. Only the signals with valid source positions (i.e. localized between the sensor positions) were used for further analysis. For the application of the pattern recognition method, the acoustic emission signal parameters (features) of both sensors were calculated from the first 100 µs of the signals after the signal arrival as described in detail in Refs. [9,13].

3. Results and discussion

We applied the pattern recognition method as described in Ref. [13] to each specimen of each stacking sequence. Representative results for two laminate configurations are shown in Fig. 2 as a diagram of the signal features Partial Power 4 over Weighted Peak Frequency. Here Partial Power 4 represents the percentage of spectral intensity between 450 kHz and 600 kHz, and the Weighted Peak Frequency is given by the square-root of Peak Frequency times Frequency Centroid [9,12,13].
Based on the different ratios of 0° and 90° plies in the three stacking sequences, different ratios of microscopic failure mechanisms are expected. As seen from Fig. 2, the absolute number of signals that correlate with matrix cracking increases with increasing number of 90° plies. Similarly, the absolute number of signals that correlate with fiber breakage increases with increasing number of 0° plies. The absolute number of signals that correlate with interfacial failure was found to be similar in all three stacking sequences. This type of signals is predominantly attributed to the occurrence of interply delamination. As the number of interfaces between 0° and 90° plies is identical in all three stacking sequences, a constant contribution is expected. The different laminate configurations cause a noticeable change in the cluster positions for each failure mechanism. This originates from changes in the frequency spectra of the excited Lamb waves caused by different elastic properties of the propagation medium and the depth changes of the acoustic emission source.

3.1. Quantification of failure mechanisms

In the following discussion, the pattern recognition results of all specimens are quantitatively evaluated according to the procedure in Ref. [9] and are shown in Fig. 3 for each specimen. In the diagram of relative numbers of signals (Fig. 3a) the contribution of matrix cracking increases as the number of 90° plies increases. Generally, a higher critical crack density is expected for $[0/90_n/0]_{sym}$ laminates for lower n before the initiation of the delamination at the interface between the 0° and 90° plies [2]. This seems to be in contrast to the quantification of matrix cracking as seen from Fig. 3a. However, the major amount of signals attributed to matrix cracking for n = 2 and n = 3 occurs after the onset of delamination and is thus not included in Nairn's theory [2]. The changes observed are thus attributed to damage occurring mostly after the onset of interply delamination.

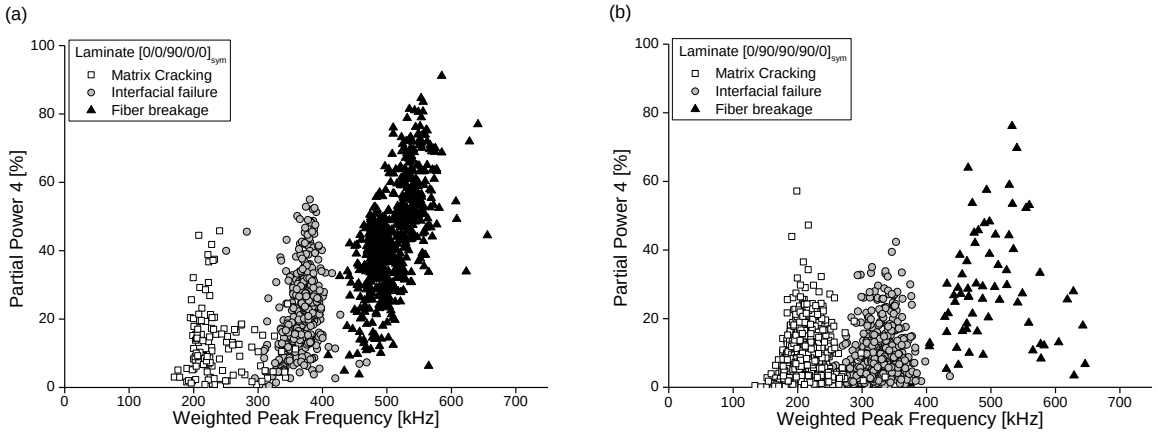

Figure 2. Representative results for the identified natural clusters for two specimens with different laminate configurations.

The number of fiber breakages increases with increasing number of 0° plies. Based on probabilistic considerations, the frequency of the occurrence of fiber breakage (i.e. single filament failure) before the ultimate failure of the specimen is expected to be proportional to the cross section of 0° plies. Contributions of interfacial failure scatter between 10% and 70%, but exhibit no significant trend as a function of stacking sequence. The large scatter of signals attributed to interfacial failure is consistent with optical observations of the macroscopic failure mode, which exhibits vast differences in the visible interply delamination surface areas.

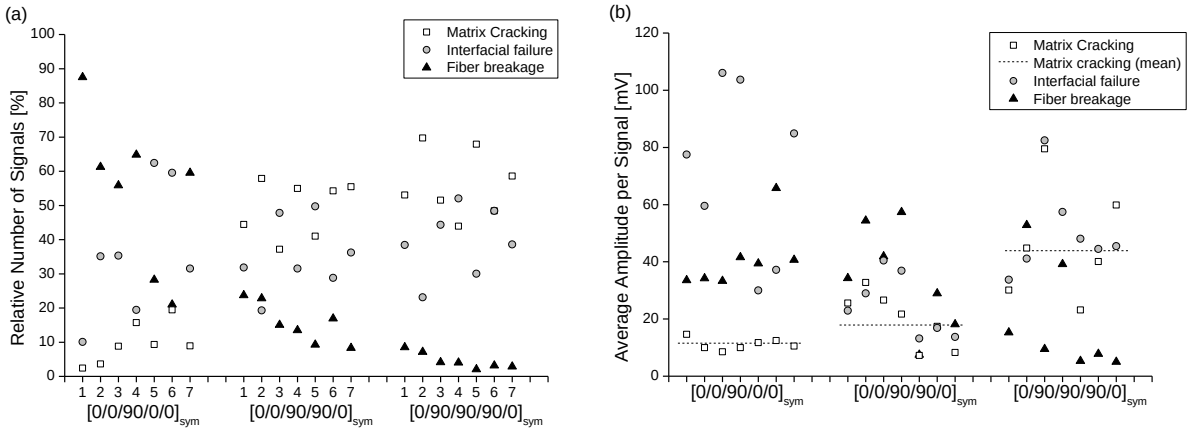

Figure 3. Quantification of relative number of signals (a) and average amplitude per signal (b) for all specimens investigated.

As predicted by the generalized theory of acoustic emission [15] and also demonstrated with finite element simulations [11], the amplitude U_{AE} of an acoustic emission signal detected at a distance r is proportional to the vibrating crack volume ΔV:

$$U_{AE} = \beta(c_L^2) \cdot \frac{\Delta V}{r} \tag{1}$$

The proportionality constant β is a linear function of the squared longitudinal sound velocity c_L of the cracking medium and the orientation of the crack surface movement (not taken into account in Eq. (1)). For the IFF case, the vibrating crack volume ΔV is expected to be proportional to the cross section area of the adjoining 90° plies. Consequently, the signal amplitudes are expected to increase by a factor of two for the $[0/0/90/90/0]_{sym}$ stacking

sequence and by a factor of three for the $[0/90/90/90/0]_{sym}$ stacking sequence, compared to the $[0/0/90/0/0]_{sym}$ stacking sequence. In Fig. 3b the average amplitude per signal is shown. The mean U_{AE} for matrix cracking (indicated by the dashed line in Fig. 3b) amounts to 11.5 mV, 17.9 mV and 43.9 mV in the three stacking sequences, respectively. Although the experimental data show some scatter, the values found are in good agreement with the expected relation based on Eq. (1). The average amplitude of the fiber breakage signals also exhibits a characteristic dependency on the stacking sequence. The mean U_{AE} decreases as the number of 0° plies decreases. As the majority of the signals belonging to this class originate from single filament failure, the vibrating crack volume is not expected to be proportional to the thickness of the adjoining 0° plies. Instead, the amplitude U_{AE} is influenced by the strain-energy release, which is higher in the stacking sequences with higher number of 0° plies.

3.2. Comparison to failure model predictions

While the diagrams of Fig. 3 are used to visualize the accumulated damage observed after the final failure of the specimens, the evolution of the microscopic failure mechanisms is of great interest for comparison to predictions from analytical failure models. Based on the values from table 1, the stress and strain values for IFF and FF (ultimate failure) were calculated for the three stacking sequences investigated according to Puck's nonlinear laminate failure model [1]. Experimentally, the stress and strain values for the onset of the three failure mechanisms were obtained from the acoustic emission measurements, and their arithmetic average was calculated from the seven samples of each stacking sequence. A graphical comparison of the obtained values, including their margin of error is shown in Fig. 4, while the respective numerical values are given in table 2.

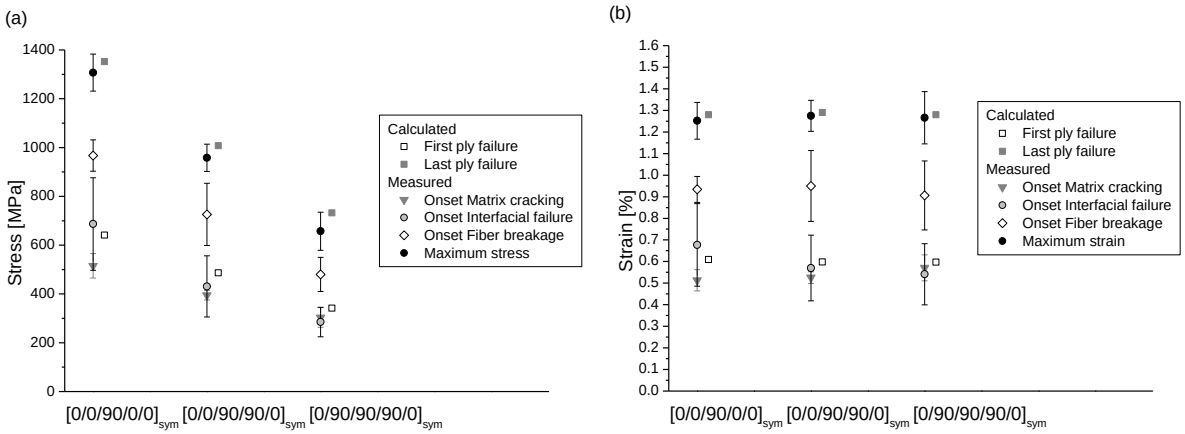

Figure 4. Calculated inter-fiber fracture and fiber fracture based on Puck's nonlinear failure model and respective values derived from acoustic emission measurements. Comparison of stress values (a) and strain values (b).

For proper usage of the FF term, distinction has to be made between the failure of single filaments and the ultimate failure of plies as introduced by the failure of fiber bundles. In the sense of the Puck failure criterion, the latter one applies. Here, the calculated stress and strain values for FF are found to be in good agreement with the measured values for maximum stress and maximum strain. In the present study, the quantified onset of fiber breakage is found to be systematically lower than the stress and strain values calculated for ultimate failure. This is explained by the fact that acoustic emission measurements are sensitive enough to detect the occurrence of single filament failure, which is expected to occur long before ultimate failure [16]. Thus, detection of fiber breakage signals by pattern recognition can effectively act as an early indicator of imminent structural failure down to a laminate

reserve factor between 0.73 and 0.76 in the current case. Good agreement is also found between the calculated stress and strain values for IFF and the initiation of matrix cracking and interfacial failure. Overall, the mean onset of matrix cracking is systematically lower than the values calculated for IFF, whereas the onset of interfacial failure is larger than the calculated value in some cases. This might be caused by acoustic emission signals originating from the edges of the specimen due to inhomogeneities and improper specimen preparation, which are easily detectable by acoustic emission measurements. Similar to the case of fiber breakage, the detection of matrix cracking and interfacial failure can be used to quantify the onset of failure in composites by acoustic emission analysis as a nondestructive measurement technique.

Laminate	Criteria	Stress [MPa]	Strain [%]
$[0/0/90/0/0]_{sym}$	interfiber fracture (Puck)	640.9	0.609
	matrix cracking	515.4 ± 50.3	0.51 ± 0.05
	interfacial failure	686.7 ± 189.6	0.68 ± 0.19
	fiber fracture (Puck)	1352.3	1.280
	fiber breakage	967.2 ± 64.5	0.93 ± 0.06
	final fracture	1307.0 ± 76.0	1.25 ± 0.09
$[0/0/90/90/0]_{sym}$	interfiber fracture (Puck)	486.4	0.598
	matrix cracking	394.8 ± 18.9	0.53 ± 0.03
	interfacial failure	431 ± 125.6	0.57 ± 0.15
	fiber fracture (Puck)	1007.73	1.290
	fiber breakage	726 ± 127.4	0.95 ± 0.16
	final fracture	958.0 ± 56.0	1.28 ± 0.07
$[0/90/90/90/0]_{sym}$	interfiber fracture (Puck)	341.8	0.597
	matrix cracking	303.9 ± 40.5	0.57 ± 0.06
	interfacial failure	285.0 ± 60.4	0.54 ± 0.14
	fiber fracture (Puck)	731.8	1.280
	fiber breakage	480.1 ± 69.9	0.91 ± 0.16
	final fracture	657.0 ± 78.0	1.27 ± 0.12

Table 2: Summary of failure model predictions and measurement results for all laminate configurations investigated.

4. Conclusion

Acoustic emission signals from tensile tests on CFRP specimens with three different stacking sequences were analyzed by pattern recognition techniques as described in [13]. The signals can be correlated to particular source mechanisms based on the results of finite element simulations as introduced previously in Refs. [11,14]. Quantification of the relative contributions of the different failure mechanisms, namely matrix cracking, interfacial failure, and fiber breakage follows the approach of Ref. [9] using the number of acoustic emission signals and their amplitude, respectively. Systematic differences are found in the number of signals originating from different failure mechanisms. The number of matrix cracks shows a systematic increase on the number of 90° plies, whereas the number of fiber breakage signals shows the opposite behavior. The number of signals correlated to interfacial failure shows no dependence on the stacking sequence, since each laminate configuration has four potential 0°/90° interfaces for initiation of delamination. The calculated average amplitudes per matrix cracking signal show strong correlation to the number of adjoined 90° plies of the stacking sequence. This is consistent with the generalized theory of acoustic emission, which predicts a strict correlation between the acoustic emission signals amplitude and the vibrating crack volume, which was found to be proportional to the cross-sectional area of the 90° plies in the current case. Furthermore, we compared the predictions of laminate failure based on Puck's nonlinear failure model and the results from acoustic emission measurements. The values for

the onset of acoustic emission signals from fiber breakage are systematically lower than the predicted FF in the 0° layers. For the current case, a prediction of ultimate failure at a reserve factor of the laminate down to 0.73 seems possible based on the detection of significant changes in the activity rate of fiber breakage signals. Within the experimental range of scatter, the onset of matrix cracking and interfacial failure was found to coincide well with the onset of the IFF predicted by Puck's nonlinear failure model.

References

[1] A. Puck, M. Mannigel, Physically based non-linear stress–strain relations for the inter-fibre fracture analysis of FRP laminates. *Composites Science and Technology*, 67(9), 1955-1964, 2007.
[2] J. A. Nairn, S. Hu, The Initiation and Growth of Delaminations Induced by Matrix Microcracks in Laminated Composites. *International Journal of Fracture*, 57, 1-24, 1992.
[3] M. J. Hinton, A. S. Kaddour, P. D. Soden. A further assessment of the predictive capabilities of current failure theories for composite laminates: comparison with experimental evidence. *Composites Science and Technology*, 64(3-4), 549-588, 2004.
[4] A. Puck, H. Schürmann, Failure Analysis of FRP Laminates by Means of Physically Based Phenomenological Models. *Composite Science and Technology*, 58, 1045-1067, 1998.
[5] M. Giordano, A. Calabro, C. Esposito, A. D'Amore, L. Nicolais. An acoustic-emission characterization of the failure modes in polymer-composite materials. *Composites Science and Technology*, 58, 1923-1928, 1998.
[6] J. Bohse. Acoustic emission characteristics of micro-failure processes in polymer blends and composites. *Composites Science and Technology*, 60, 1213-1226, 2000.
[7] S. Huguet, N. Godin, R. Gaertner, L. Salmon, D. Villard. Use of acoustic emission to identify damage modes in glass fibre reinforced polyester. *Composites Science and Technology*, 62, 1433-1444, 2002.
[8] C. R. Ramirez-Jimenez, N. Papadakis, N. Reynolds, T. Gan, P. Purnell, M. Pharaoh. Identification of failure modes in glass/polypropylene composites by means of the primary frequency content of the acoustic emission event. *Composites Science and Technology*, 64, 1819-1827, 2004.
[9] M. G. R. Sause, T. Müller, A. Horoschenkoff, S. Horn. Quantification of failure mechanisms in mode-I loading of fiber reinforced plastics utilizing acoustic emission analysis. *Composite Science and Technology*, 72, 167-174, 2012.
[10] A. Marec, J.-H. Thomas, R. Guerjouma. Damage characterization of polymer-based composite materials: Multivariable analysis and wavelet transform for clustering acoustic emission data. *Mechanical Systems and Signal Processing*, 22, 1441-1464, 2008.
[11] M. G. R. Sause, S. Horn. Simulation of acoustic emission in planar carbon fiber reinforced plastic specimens. *Journal of Nondestructive Evaluation*, 29(2), 123-142, 2010.
[12] M. A. Hamstad, A. O'Gallagher, J. Gary. A Wavelet Transform Applied To Acoustic Emission Signals: Part 1: Source Identification. *Journal of Acoustic Emission*, 20, 39-61 2002.
[13] M. G. R. Sause, A. Gribov, A. R. Unwin, S. Horn. Pattern recognition approach to identify natural clusters of acoustic emission signals. *Pattern Recognition Letters*, 33(1), 17-23, 2012.
[14] M. G. R. Sause, M. A. Hamstad, S. Horn**.** Finite element modeling of conical acoustic emission sensors and corresponding experiments. *Sensors and Actuators A: Physical*, 184, 64-71, 2012.
[15] M. Ohtsu, K. Ono. The generalized theory and source representation of acoustic emission. *Journal of Acoustic Emission*, 5, 124-133, 1986.
[16] A.E. Scott, M. Mavrogordato, P. Wright, I. Sinclair, S.M. Spearing. In situ fibre fracture measurement in carbon–epoxy laminates using high resolution computed tomography. *Composites Science and Technology*, 71, 1471-1477, 2011.